

Asymptotic Exceptional Steady States in Dissipative Dynamics

Yu-Min Hu¹ and Jan Carl Budich^{1,2,*}

¹Max Planck Institute for the Physics of Complex Systems, Nöthnitzer Str. 38, 01187 Dresden, Germany

²Institute of Theoretical Physics, Technische Universität Dresden and
Würzburg-Dresden Cluster of Excellence ct.qmat, 01062 Dresden, Germany

Spectral degeneracies in Liouvillian generators of dissipative dynamics generically occur as exceptional points, where the corresponding non-Hermitian operator becomes non-diagonalizable. Steady states, i.e. zero-modes of Liouvillians, are considered a fundamental exception to this rule since a no-go theorem excludes non-diagonalizable degeneracies there. Here, we demonstrate in the context of dissipative state preparation how a system may asymptotically approach the forbidden scenario of an exceptional steady state in the thermodynamic limit. Building on case studies ranging from NP-complete satisfiability problems encoded in a quantum master equation to the dissipative preparation of a symmetry protected topological phase, we reveal the close relation between the computational complexity of the problem at hand, and the finite size scaling towards the exceptional steady state, exemplifying both exponential and polynomial scaling. Treating the strength W of quantum jumps in the Lindblad master equation as a parameter, we show that exceptional steady states at the physical value $W = 1$ may be understood as a critical point hallmarking the onset of dynamical instability.

Quantum state preparation remains a formidable challenge with implications reaching far beyond its natural habitat of quantum science. In particular, the solution to hard problems of general interest such as NP-complete satisfiability (SAT) problems [1–3] and their quantum counterparts known as QMA-complete problems [4–6] may be readily viewed as quantum state preparation tasks, e.g. solved by preparing the ground state of a suitable local Hamiltonian in a quantum simulator [7–10]. Among the merits of extensive research on coherent approaches such as adiabatic quantum computing are recipes to encode the solution to a computational problem in the ground state of a local parent Hamiltonian [11–13]. This may offer valuable insights even if the path to the ground state is obstructed by a (discontinuous) quantum phase transition entailing (exponential) critical slowdown [14–20].

Dissipative state preparation aims at addressing this challenge by considering incoherent processes as a resource for designing a quantum master equation [21–34]. That way a targeted many-body state is approached largely independent of initial conditions as the steady state of the open system dynamics. In this context, a central equation of motion is the Lindblad master equation [35, 36]

$$\frac{d}{dt}\rho = \mathcal{L}_W[\rho] = -i(H_{\text{NH}}\rho - \rho H_{\text{NH}}^\dagger) + W \sum_{\mu} L_{\mu}\rho L_{\mu}^\dagger, \quad (1)$$

governing the dynamics of the density matrix ρ of a system weakly coupled (Born) to a bath with negligible memory (Markov). Incoherent processes reflecting the influence of the bath are described by quantum jump operators L_{μ} , while $H_{\text{NH}} = H - (i/2)\sum_{\mu} L_{\mu}^\dagger L_{\mu}$ is the effective non-Hermitian (NH) Hamiltonian combining the Hermitian system Hamiltonian H (as in the Schrödinger equation of a closed system) with the anti-Hermitian damping enacted by the bath. We emphasize that the coupling strength W of the quantum jump term is physically fixed to $W = 1$, but for our subsequent analysis, it will be fruitful to consider W as a parameter, which amounts to postselection of quantum trajectories [37–41]. Steady states are zero modes of the Liouvillian $\mathcal{L}_{W=1}$, and

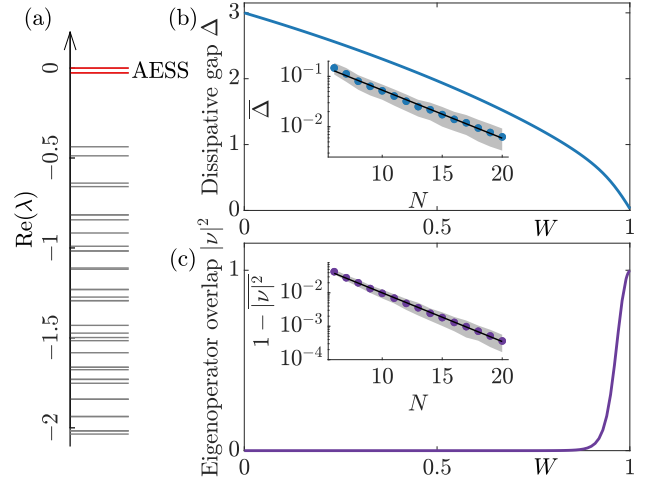


FIG. 1. (a) Liouvillian spectrum ($W = 1$ in Eq. (1)) for a satisfiable 3SAT instance with a unique solution, $N = 14$ variables, and $M = \text{round}(\alpha_c N)$ clauses, where the satisfiability threshold $\alpha_c \approx 4.267$. The two red states form the asymptotic exceptional steady state (AESS). (b,c) Liouvillian gap Δ and eigenoperator overlap $|v|^2$ as a function of W (other parameters as in (a)). The insets in (b,c) show the mean values of Δ and $|v|^2$ at $W = 1$ change with the number of variables N , averaging over 10^3 random instances for each N with $M = \text{round}(\alpha_c N)$. All instances have a unique solution. Shadow regions indicate the standard deviation among instances.

a dissipative counterpart of critical slowdown is an (asymptotic) degeneracy of the steady state [cf. Fig. 1(a)]. Importantly, while degeneracies generically occur in the form of non-diagonalizable (or exceptional) points (EP) for NH operators [42–47], such as Liouvillian exceptional points [48–56], a rigorous no-go theorem excludes this possibility for degenerate steady states [57].

Here, we demonstrate how a system may asymptotically approach the forbidden scenario of a steady state EP in the thermodynamic limit at the physical value $W = 1$ (see Fig. 1 for a paradigmatic example). Interestingly, we find that the

finite size scaling of such *asymptotic exceptional steady state* (AESS) is directly linked to the computational complexity of the state preparation task at hand. Specifically, for the NP-complete 3SAT problem (cf. Fig. 1) the AESS is approached exponentially in system size N . Moreover, for a Lindbladian with a symmetry-protected topological phase as a steady state, we find that an AESS is approached with polynomial scaling, reflecting the continuous topological quantum phase transition separating the steady state from a trivial initial state in symmetry-preserving dynamics [cf. Fig. 3(c) below]. Our findings are further elucidated by considering $W \neq 1$, where an exact exceptional point is found at the onset of dynamical instability at a value $W_c > 1$ which approaches the physical value $W = 1$ with a similar finite size scaling as the Liouvillian gap (see Fig. 2). Conversely, for $W < 1$, we may continuously approach the conceptually simplest dissipative dynamics obtained by neglecting the jump term ($W = 0$) and only considering the deterministic non-unitary dynamics generated by H_{NH} . While the finite Liouvillian gap at $W = 0$ [see Fig. 1(b)] suggests convergence to the solution in a time scaling linearly in system size, we emphasize that a direct experimental implementation of $W = 0$ requires post-selection of processes (quantum trajectories) without quantum jump events, the probability of which is attenuated exponentially over time.

Dissipative state preparation.—The central idea of this state preparation paradigm is to target a pure state $\rho_t = |\psi_t\rangle\langle\psi_t|$ by encoding it into the steady-state subspace of a physical open quantum system, i.e., $\mathcal{L}_1[\rho_t] = 0$. In our present approach, we set $H = 0$ for simplicity and consider jump operators of the form $L_\mu = O_\mu P_\mu$. Here, the projector P_μ satisfies $P_\mu |\psi_t\rangle = 0$ and the operator O_μ maps unwanted states into the subspace containing $|\psi_t\rangle$. In other words, $|\psi_t\rangle$ lies in the decoherence-free subspace [58] while jump operators dissipate undesirable states. These jump operators lead to an anti-Hermitian effective Hamiltonian

$$H_{\text{NH}} = -(i/2) \sum_{\mu} P_{\mu} O_{\mu}^{\dagger} O_{\mu} P_{\mu} = -iH', \quad (2)$$

such that $|\psi_t\rangle$ is a frustration-free ground state of the Hermitian H' . At $W = 0$, $\mathcal{L}_0[\rho] = -(H', \rho)$ generates the imaginary time evolution of H' [59, 60].

A key quantity to characterize critical slowdown is the relaxation time τ , which is determined by the Liouvillian spectrum. A diagonalizable Liouvillian \mathcal{L}_W satisfies $\mathcal{L}_W[r_i] = \lambda_i r_i$ and $\mathcal{L}_W^{\dagger}[l_i] = \lambda_i^* l_i$, respectively. Here, λ_i is the i th eigenvalue, ordered by their real parts $\text{Re}(\lambda_0) \geq \text{Re}(\lambda_1) \geq \text{Re}(\lambda_2) \geq \dots \geq \text{Re}(\lambda_{D^2-1})$, where D is the Hilbert space dimension, and r_i (l_i) are the right (left) eigenoperators, whose Hilbert-Schmidt inner product satisfies the biorthonormal relation $\text{Tr}[l_i^{\dagger} r_j] = \delta_{ij}$. At the physical point ($W = 1$), the eigenmodes with $\lambda_i = 0$ correspond to the steady-state subspace. Unless explicitly stated otherwise, we will assume a unique steady state of \mathcal{L}_1 throughout the text. Thus, $\lambda_0 = 0$ and $\text{Re}(\lambda_1) < 0$ at $W = 1$. Consequently, it is the Liouvillian gap $\Delta = |\text{Re}(\lambda_0 - \lambda_1)|$ that reveals the relaxation time $\tau \sim \Delta^{-1}$.

Dissipative 3SAT solver.—To reveal the presence of AESS,

we first consider the NP-complete 3SAT problem. With N Boolean variables x_1, x_2, \dots, x_N , we define M disjunction clauses, each containing three variables or their negations (e.g., $C_m = x_{m_1} \vee \neg x_{m_2} \vee x_{m_3}$). The 3SAT problem asks whether a conjunction of clauses $C_1 \wedge C_2 \wedge \dots \wedge C_M$ can be satisfied by assigning TRUE (1) or FALSE (0) to each binary variable. By mapping TRUE and FALSE of a variable x_n to the states $|1\rangle$ and $|0\rangle$ of a qubit σ_n , the 3SAT problem is converted into finding the ground state of a 3-local Ising-like Hamiltonian $H_{3\text{SAT}} = \sum_{m=1}^M P_m$ [61]. The projector P_m acts on three qubits involved in clause C_m and assigns a unit energy penalty to unsatisfied clauses. For example, $C_m = x_{m_1} \vee \neg x_{m_2} \vee x_{m_3}$ corresponds to $P_m = (1 - \sigma_{m_1}^z)(1 + \sigma_{m_2}^z)(1 - \sigma_{m_3}^z)/8$ which punishes the configuration $|010\rangle$ of the three participating variables. Here, $\sigma_n^{x,y,z}$ are Pauli operators for the n th qubit, with $\sigma_n^z |1\rangle = |1\rangle$ and $\sigma_n^z |0\rangle = -|0\rangle$. As a result, the solution to a satisfiable 3SAT instance is encoded in a zero-energy ground state $|\psi_{\text{sol}}\rangle$ of $H_{3\text{SAT}}$, where $P_m |\psi_{\text{sol}}\rangle = 0$ and $|\psi_{\text{sol}}\rangle$ represents a bit string. This maps the problem to the standard state preparation task of preparing the ground states of a target Hamiltonian $H_{3\text{SAT}}$. Yet, the NP-complete nature of 3SAT indicates the generic hardness of completing this task.

To harness the dissipative state preparation framework, we design dissipative processes for each clause C_m through three jump operators:

$$L_{m,\alpha} = \sigma_{m_\alpha}^x P_m, \quad \alpha = 1, 2, 3. \quad (3)$$

These $L_{m,\alpha}$ dissipate the unsatisfiable configuration of clause C_m and rotate qubit m_α into its satisfiable subspace. As a result, the solution to a satisfiable 3SAT instance is given by the steady state $r_0 = |\psi_{\text{sol}}\rangle\langle\psi_{\text{sol}}|$ of the corresponding \mathcal{L}_1 . Remarkably, Eq. (3) leads to $H' = 3H_{3\text{SAT}}/2$ [cf. Eq. (2)], indicating that the imaginary time evolution of $H_{3\text{SAT}}$ is achieved by $\mathcal{L}_{W=0}$. While the evolution of \mathcal{L}_0 approaches $|\psi_{\text{sol}}\rangle$ at a finite timescale due to a finite (and constant with N) gap of $H_{3\text{SAT}}$ [Fig. 1(b)], the hardness of the 3SAT problem hides in post-selecting an exponentially small portion among all quantum trajectories to effectively realize $W = 0$. An interesting question is: How does the complexity of 3SAT problem manifest in the spectrum of \mathcal{L}_W as a function of W , in particular at the natural physical value $W = 1$?

To examine the spectrum of \mathcal{L}_W for the dissipative 3SAT solver, we consider satisfiable 3SAT instances with a unique solution for simplicity and leave the case with multiple solutions to the supplemental material [62, 63]. Hard satisfiable instances are generated using the method from Ref. [64]. The clause-to-variable ratio M/N is set to the satisfiability threshold $\alpha_c \approx 4.267$, below (above) which a generic instance is satisfiable (unsatisfiable) [3]. With $H = 0$, the jump operators in Eq. (3) decouple the dynamics of diagonal and off-diagonal parts of ρ in the computational basis spanned by $|i\rangle$ for the i th bit string. Because the steady state $r_0 = |\psi_{\text{sol}}\rangle\langle\psi_{\text{sol}}|$ lives in the diagonal part and off-diagonal terms decay at a finite timescale, we may effectively consider classical dynamics occurring in the 2^N -dimensional diagonal operator subspace formed by the basis $|i\rangle \equiv |i\rangle\langle i|$ [62]. Under these cir-

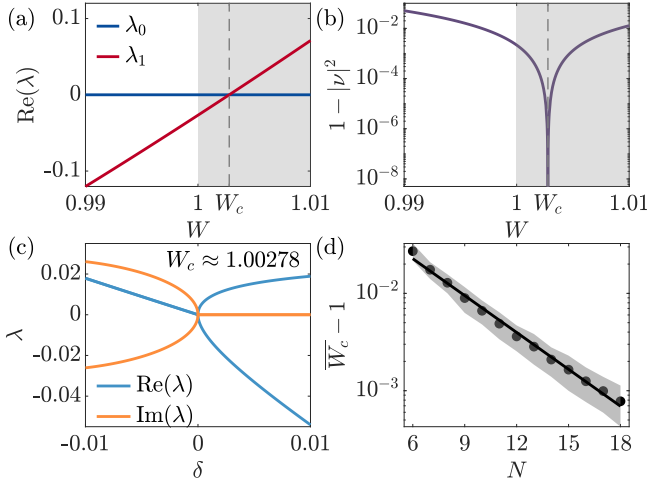


FIG. 2. Eigenvalues (a) of steady and metastable states and their eigenoperator overlap (b) over W [same instance as in Fig. 1]. The shaded region represents $W > 1$, where $\text{Re}(\lambda_1) > 0$ renders the system dynamically unstable in the thermodynamic limit. We observe an EP at $W_c \approx 1.00278$. (c) Perturbed eigenvalues for $\mathcal{L}_{W_c} + \mathcal{L}_{W_c}^{\text{pert}}$, where δ is the perturbation strength. (d) The mean W_c decays with N . Each point is averaged over 10^3 instances with one solution and the shaded region marks the standard deviation between instances.

cumstances, the computational effort behind solving \mathcal{L}_W is reduced treating a smaller superoperator of dimension 2^N , and our numerical data in Figs 1 and 2 are based on this (exact) simplification. Nevertheless, we note that our analysis applies to both classical and quantum systems, and genuine quantum terms will be considered further below.

The spectrum of \mathcal{L}_1 for a typical satisfiable instance is presented in Fig. 1(a). Besides the steady state $r_0 = |\psi_{\text{sol}}\rangle\langle\psi_{\text{sol}}|$, we observe a metastable state r_1 that is well-separated from other damping modes, whose eigenvalue is close to zero. As shown in Fig. 1(b), this metastable state provides a small Liouvillian gap at $W = 1$, in contrast to the finite gap at the imaginary time evolution point $W = 0$. Importantly, the mean Liouvillian gap $\overline{\Delta}$ at $W = 1$, averaged over 10^3 satisfiable instances, exhibits an exponential decay as N increases, indicating that the dissipative 3SAT solver takes an exponentially long time to find a solution.

The most interesting result appears in the eigenoperator overlap ν between steady and metastable states:

$$\nu = \text{Tr}[\hat{r}_0^\dagger \hat{r}_1], \quad (4)$$

where we define the normalized eigenoperators $\hat{r}_i = r_i / \|r_i\|$ with the Hilbert-Schmidt norm $\|r\| = \sqrt{\text{Tr}[\rho^\dagger \rho]}$. $|\nu|^2 = 0$ ($|\nu|^2 = 1$) reveals these two states are orthogonal (parallel) to each other. As shown in Fig. 1(c), we find that $|\nu|^2 = 0$ at $W = 0$, as the two eigenoperators correspond to eigenstates of a Hermitian Hamiltonian $H_{3\text{SAT}}$. However, $|\nu|^2$ grows to a value that is extremely close to 1 at $W = 1$. The inset of Fig. 1(c) further demonstrates that the averaged quantity $1 - |\nu|^2$ at $W = 1$ decays exponentially as N increases.

Asymptotic exceptional steady state.—These numerical findings imply that the metastable and steady states asymptotically approach an EP in the thermodynamic limit ($N \rightarrow +\infty$), where both their eigenvalues and eigenoperators asymptotically coalesce, dubbed the asymptotic exceptional steady state (AESS). While a no-go theorem rules out the possibility of the steady state belonging to any EP subspace [57], the observed AESS offers an unexpected case to systematically approach, yet not break, the boundary of this fundamental limitation.

We note that, in a finite system, an exponentially small finite Liouvillian gap at $W = 1$ prevents two nearly degenerate states from becoming an exact EP. However, a slight increase of W to a critical value $W_c > 1$ makes $\Delta = 0$ and $|\nu|^2 = 1$, indicating that these two states coalesce to become an exact EP in an extended parameter space [Fig. 2(a-b)]. Notably, the EP at $W = W_c$ signifies a phase transition into a dynamically unstable region where $\lambda_1 > 0$ and the steady state becomes ill-defined [65]. Moreover, we observe that the critical value W_c converges to 1 in the thermodynamic limit, whose mean deviation $\overline{W}_c - 1$ is compatible with an exponential decay with increasing system size [Fig. 2(d)]. All these results demonstrate that the physical AESS at $W = 1$ is extremely close to an exact EP.

We now develop an effective theory to describe the AESS. When $W \neq W_c$, an orthonormal operator basis between r_0 and r_1 can be constructed: $\tilde{r}_0 = \hat{r}_0$ and $\tilde{r}_1 = (\hat{r}_1 - \nu \hat{r}_0) / (1 - |\nu|^2)^{1/2}$, in which the Liouvillian superoperator becomes

$$\mathcal{L}_W^{\text{eff}} = \begin{pmatrix} 0 & \lambda_1 \frac{\nu}{\sqrt{1-|\nu|^2}} \\ 0 & \lambda_1 \end{pmatrix}. \quad (5)$$

Therefore, when $\lambda_1 \rightarrow 0$ and $|\nu|^2 \rightarrow 1$ are simultaneously achieved by either taking the thermodynamic limit or setting $W \rightarrow W_c$, the effective 2-by-2 matrix $\mathcal{L}_W^{\text{eff}}$ asymptotically approaches the Jordan-block structure of an EP. Clearly, the Liouvillian gap and eigenoperator overlap play separate roles in the coalescence of the eigenvalues and eigenstates of the AESS. This structure rules out the possibility of an open quantum system at $W = 1$ approaching the AESS when only one of the limits $\Delta \rightarrow 0$ and $|\nu|^2 \rightarrow 1$ is achieved [62].

To further demonstrate that the AESS at $W = 1$ is near an exact EP at $W = W_c$, we perturb the spectrum of \mathcal{L}_W by adding a perturbative Liouvillian $\mathcal{L}_W^{\text{pert}}[\rho] = \delta \sum_{n=1}^N (W L_n \rho L_n^\dagger - \frac{1}{2} \{L_n^\dagger L_n, \rho\})$ with $L_n = \sigma_n^-$, where δ is the perturbation strength. Since a solution $|\psi_{\text{sol}}\rangle$ to a random satisfiable instance is unlikely to be a dark state for all $L_n = \sigma_n^-$, this perturbation erases the solution in the steady state. While a physical dissipative dynamics requires $\delta > 0$ and $W = 1$, we mathematically consider both $\delta > 0$ and $\delta < 0$ at $W = W_c > 1$. As shown in Fig. 2(c), the perturbed eigenvalues are purely real when $\delta > 0$ and form complex-conjugated pairs when $\delta < 0$, undergoing a parity-time symmetry breaking at $\delta = 0$ [66–69]. This is a clear signature of an exact EP at $\delta = 0$ and $W = W_c$.

We now go back to the physical value $W = 1$. Although a finite-size gap prevents a similar perturbative analysis, the AESS still plays a crucial role in the complexity

of state preparation tasks at hand. With the biorthonormal relation $\text{Tr}[l_i^\dagger r_j] = \delta_{ij}$ for \mathcal{L}_1 , an initial density matrix ρ_{ini} follows the time evolution $\rho(t) = r_0 + \sum_{i \geq 1} e^{\lambda_i t} c_i r_i$ where $c_i = \text{Tr}[l_i^\dagger \rho_{\text{ini}}]$. In Fig. 1(a), $|\text{Re}(\lambda_1)| \ll |\text{Re}(\lambda_2)|$ indicates a separation of timescales. Specifically, when $|\text{Re}(\lambda_2)|^{-1} \ll t \ll |\text{Re}(\lambda_1)|^{-1}$, the evolution effectively occurs between metastable and steady states: $\rho(t) = r_0 + e^{\lambda_1 t} c_1 r_1 + o(e^{\lambda_2 t})$.

To reveal the role of AESS in relaxation dynamics, we further investigate the eigenoperators l_1 and r_1 . Recalling that $r_0 = |\psi_{\text{sol}}\rangle\langle\psi_{\text{sol}}|$ is a projector and $l_0 = I$ is the identity, the biorthonormal relations $\text{Tr}[l_0^\dagger r_1] = \text{Tr}[l_1^\dagger r_0] = 0$ give rise to $\text{Tr}[r_1] = 0$ and $\langle l_1 \rangle = 0$, where we define $\langle \cdot \rangle = \text{Tr}[r_0^\dagger (\cdot)] = \langle \psi_{\text{sol}} | \cdot | \psi_{\text{sol}} \rangle$. The presence of AESS indicates that r_1 is close to r_0 . We thus decompose r_1 as $r_1 = \langle r_1 \rangle r_0 + \delta_r$. The deviation δ_r is orthogonal to r_0 under Hilbert-Schmidt inner product, satisfying $\langle \delta_r \rangle = 0$. The biorthonormal relation $\text{Tr}[l_1^\dagger r_1] = 1$ leaves freedom to choose the normalization $\|r_1\|$. We take $\langle r_1 \rangle = 1$, which leads to $r_1 = r_0 + \delta_r$ with $\text{Tr}[\delta_r] = -1$. With these properties, Eq. (4) provides $\|\delta_r\|^2 = \text{Tr}[\delta_r^\dagger \delta_r] = 1 - |\nu|^{-2}$, indicating that the correction δ_r (and its norm) asymptotically vanishes in a large system with AESS. Similarly for l_1 , provided that $\langle l_1^\dagger \rangle = 0$, we take the ansatz $l_1 = \kappa(I - r_0) + \delta_l$ where $\langle \delta_l \rangle = \text{Tr}[\delta_l] = 0$ and $\kappa = \text{Tr}[l_1]/(2^N - 1)$. The relation $\text{Tr}[l_1^\dagger r_1] = 1$ leads to $\text{Tr}[\delta_l^\dagger \delta_r] = 1 + \kappa$. We then calculate the eigenoperator overlap between l_0 and l_1 : $|\nu|^2 = \frac{|\text{Tr}[l_0^\dagger l_1]|^2}{\|l_0\|^2 \|l_1\|^2} = (1 - \frac{1}{2^N})(1 - \frac{\|\delta_l\|^2}{\|l_1\|^2})$. Since an AESS indicates $|\nu|^2 \rightarrow 1$, we get $\frac{\|\delta_l\|^2}{\|l_1\|^2} \rightarrow 0$ as the system size increases. Thus, $\|\delta_l\|$ may also be viewed as a small correction relative to the extensive operator $\kappa(I - r_0)$.

With this structure of r_1 and l_1 , we investigate the long-time dynamics $\rho(t) = r_0 + e^{\lambda_1 t} c_1 r_1 + o(e^{\lambda_2 t})$. Since $c_1 = \text{Tr}[l_1^\dagger \rho_{\text{ini}}]$ and l_1 is close to a projector $I - |\psi_{\text{sol}}\rangle\langle\psi_{\text{sol}}|$, a random initial state will typically lead to a nonzero c_1 , therefore requiring an exponentially long time $\tau \sim |\text{Re}(\lambda_1)|^{-1}$ to approach the solution state $|\psi_{\text{sol}}\rangle$. One possible way to accelerate the relaxation dynamics is to carefully choose an initial state such that $c_1 = 0$, which would lead to a much shorter relaxation time $\tau' \sim |\text{Re}(\lambda_2)|^{-1}$ [70]. However, in the dissipative 3SAT solver, we numerically find that $\kappa^{-1}l_1$ is positive semidefinite, with a single zero eigenvalue corresponding to the eigenstate $|\psi_{\text{sol}}\rangle$ separated by a gap that is constant in N [62]. This numerical finding seems to exclude the possibility of finding easily accessible initial states ρ_{ini} such that $c_1 = 0$, as the only solution would be to (tautologically) start from the target state $r_0 = |\psi_{\text{sol}}\rangle\langle\psi_{\text{sol}}|$. Based on this evidence, we argue that the appearance of AESS, which leads to an approximate projector structure of l_1 , is directly connected to the complexity of dissipative state preparation tasks.

Quantum AESS.— While the above dissipative 3SAT solver is governed by classical dynamics, the analysis of AESS also applies to genuine quantum dynamics. To corroborate this, we provide two interesting quantum examples: a modified dissipative 3SAT solver with quantum terms, and a dissipative protocol for preparing the celebrated Affleck–Kennedy–Lieb–Tasaki (AKLT) state [71].

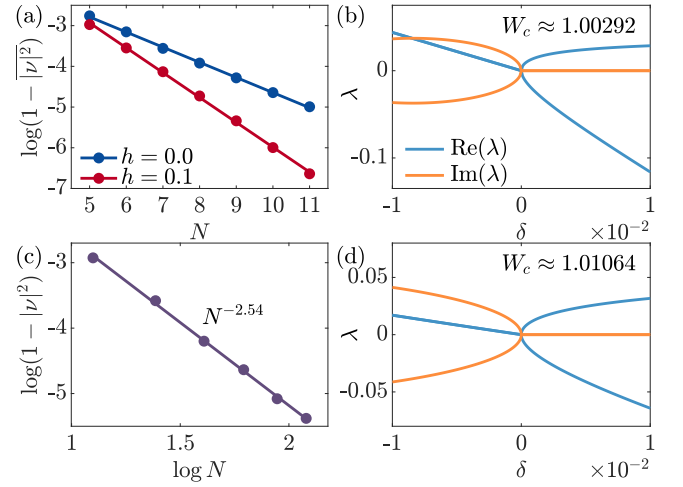


FIG. 3. AESS in quantum systems. (a) The case of including a modified transverse field [Eq. (6)] in dissipative 3SAT solver. We set $M = \text{round}(\alpha_c N)$ and $W = 1$. All points are obtained by averaging over 10^3 satisfiable instances with a unique solution. (b) The perturbed eigenvalues of $\mathcal{L}_{W_c} + \mathcal{L}_{W_c}^{\text{pert}}$ for a uniquely solvable 3SAT instance with $N = 11$. (c) Eigenoperator overlap of \mathcal{L}_1 for preparing the AKLT state [Eq. (7)]. (d) The perturbed eigenvalues of $\mathcal{L}_{W_c} + \mathcal{L}_{W_c}^{\text{pert}}$ for AKLT state preparation with $N = 7$.

In the modified dissipative 3SAT solver, we add a quantum Hamiltonian H_X to the dissipative dynamics in Eq. (3):

$$H_X = h \sum_{m \neq m'}^M \sum_{n \in \text{Ind}_{m,m'}} P_{m,m'} \sigma_n^x P_{m,m'} \quad (6)$$

where $P_{m,m'} = I - (I - P_m)(I - P_{m'})$, h is the interaction strength, and $\text{Ind}_{m,m'}$ contains the qubit indexes involved in clauses C_m and $C_{m'}$. This Hamiltonian describes a modified transverse field that only generates dynamics in the subspace orthogonal to $|\psi_{\text{sol}}\rangle\langle\psi_{\text{sol}}|$. Therefore, $|\psi_{\text{sol}}\rangle\langle\psi_{\text{sol}}|$ is still the steady state at $W = 1$. A similar numerical investigation [Fig. 3(a)] as for the classical case indicates that the AESS still exists in quantum dynamics, where both the eigenvalues and eigenoperators of steady and metastable states for \mathcal{L}_1 coalesce in the thermodynamic limit. Additionally, an exact EP will appear at a slightly larger $W = W_c > 1$, which is confirmed by the perturbed eigenvalues [Fig. 3(b)] at $W = W_c$ after adding a perturbation $\mathcal{L}_{W_c}^{\text{pert}}[\rho] = \delta \sum_{n=1}^N (W_c L_n \rho L_n^\dagger - \frac{1}{2} (L_n^\dagger L_n, \rho))$ with $L_n = \sigma_n^x$.

Both 3SAT solvers eventually stabilize a classical steady state. We now demonstrate that an AESS can also occur as a nontrivial quantum state. This can be seen in the dissipative state preparation of symmetry-protected topological states such as the AKLT state [21, 31, 72]. We consider a one-dimensional $S = 1$ spin system ($H = 0$) with four types of jump operators:

$$L_{n,\alpha} = S_n^a P_{n,n+1}^{(2)}, \quad L'_{n,\alpha} = S_{n+1}^a P_{n,n+1}^{(2)}, \quad (7)$$

where $\alpha = x, y, z$. $S_n^{x,y,z}$ are spin-1 operators. $P_{n,n+1}^{(2)}$ projects two neighboring $S = 1$ spins into the $S = 2$ subspace

[71]. We assume that there are N spins and take periodic boundary conditions $S_1 = S_{N+1}$. By construction, the AKLT state $|\psi_{\text{AKLT}}\rangle$ lives in the decoherence-free subspace since $P_{n,n+1}^{(2)}|\psi_{\text{AKLT}}\rangle = 0$ for $n = 1, \dots, N$, thus giving the steady state $|\psi_{\text{AKLT}}\rangle\langle\psi_{\text{AKLT}}|$ of \mathcal{L}_1 . We find that the AESS still exists at $W = 1$ [Fig. 3(c)] and is close to an exact EP at a slightly larger $W = W_c > 1$. We also perturb the exact EP by adding a perturbative Liouvillian $\mathcal{L}_{W_c}^{\text{pert}}[\rho] = \delta \sum_{n=1}^N (W_c L_n \rho L_n^\dagger - \frac{1}{2} \{L_n^\dagger L_n, \rho\})$ with $L_n = S_n^z$. The perturbed eigenvalues [Fig. 3(d)] elucidate the spectral EP structure.

Interestingly, the eigenoperator overlap $1 - |\nu|^2$ in Fig. 3(c) decays as a power-law with increasing system size, distinct from the exponential decay observed in Figs. 1 and 3(a) for 3SAT. These numerical findings further corroborate the close relation between the finite-size scaling of the AESS and the complexity of preparing target states. Preparing a symmetry-protected topological state in a symmetry preserving fashion requires a polynomial time reflecting the obstruction by a continuous topological quantum phase transition, while an exponentially long time is expected to be required to solve the NP-complete 3SAT problem.

Discussion.— We have revealed the existence of asymptotic exceptional steady states and discussed its intriguing connection to the computational complexity of state preparation tasks. The AESS is found to be near an exact EP in an extended parameter space and to play a vital role in relaxation dynamics to target states. An important future question is to put AESS on a rigorous mathematical ground by determining the precise conditions for its appearance in open quantum many-body systems. Furthermore, an interesting direction is to identify Hamiltonian or dissipative perturbations that are compatible with the targeted steady state but mitigate the scaling behavior of the AESS so as to speed up the state preparation task. Such perturbations may be seen as a dissipative counterpart to quantum catalysts in adiabatic quantum computing [13].

Acknowledgment.— We thank Emil J. Bergholtz, Sebastian Diehl, Tim Pokart, Joachim Schwardt, and Grigori Starkov for helpful discussions. JCB acknowledges financial support from the German Research Foundation (DFG) through the Collaborative Research Centre SFB 1143 (Project-ID 247310070), and the Cluster of Excellence ct.qmat (Project-ID 390858490).

Note added.— While preparing this manuscript for submission, we became aware of a somewhat related preprint [73] which discusses Liouvillian EPs in a few-level system with $W \neq 1$, but without relating to the large N phenomenon of AESS introduced in our present work.

* jan.budich@tu-dresden.de

[1] S. A. Cook, The complexity of theorem-proving procedures, in *Logic, automata, and computational complexity: The works of Stephen A. Cook* (2023) pp. 143–152.

- [2] R. M. Karp, Reducibility among combinatorial problems, in *50 Years of Integer Programming 1958-2008: from the Early Years to the State-of-the-Art* (Springer, 2009) pp. 219–241.
- [3] M. Mézard and R. Zecchina, Random k -satisfiability problem: From an analytic solution to an efficient algorithm, *Phys. Rev. E* **66**, 056126 (2002).
- [4] A. Y. Kitaev, A. Shen, and M. N. Vyalyi, *Classical and quantum computation*, 47 (American Mathematical Soc., 2002).
- [5] J. Kempe, A. Kitaev, and O. Regev, The complexity of the local hamiltonian problem, *Siam journal on computing* **35**, 1070 (2006).
- [6] D. Aharonov, W. Van Dam, J. Kempe, Z. Landau, S. Lloyd, and O. Regev, Adiabatic quantum computation is equivalent to standard quantum computation, *SIAM review* **50**, 755 (2008).
- [7] I. Buluta and F. Nori, Quantum simulators, *Science* **326**, 108 (2009).
- [8] J. I. Cirac and P. Zoller, Goals and opportunities in quantum simulation, *Nature physics* **8**, 264 (2012).
- [9] I. M. Georgescu, S. Ashhab, and F. Nori, Quantum simulation, *Rev. Mod. Phys.* **86**, 153 (2014).
- [10] A. J. Daley, I. Bloch, C. Kokail, S. Flannigan, N. Pearson, M. Troyer, and P. Zoller, Practical quantum advantage in quantum simulation, *Nature* **607**, 667 (2022).
- [11] E. Farhi, J. Goldstone, S. Gutmann, J. Lapan, A. Lundgren, and D. Preda, A quantum adiabatic evolution algorithm applied to random instances of an np-complete problem, *Science* **292**, 472 (2001).
- [12] A. Das and B. K. Chakrabarti, Colloquium: Quantum annealing and analog quantum computation, *Rev. Mod. Phys.* **80**, 1061 (2008).
- [13] T. Albash and D. A. Lidar, Adiabatic quantum computation, *Rev. Mod. Phys.* **90**, 015002 (2018).
- [14] A. P. Young, S. Knysh, and V. N. Smelyanskiy, First-order phase transition in the quantum adiabatic algorithm, *Phys. Rev. Lett.* **104**, 020502 (2010).
- [15] T. Jörg, F. Krzakala, G. Semerjian, and F. Zamponi, First-order transitions and the performance of quantum algorithms in random optimization problems, *Phys. Rev. Lett.* **104**, 207206 (2010).
- [16] B. Altshuler, H. Krovi, and J. Roland, Anderson localization makes adiabatic quantum optimization fail, *Proceedings of the National Academy of Sciences* **107**, 12446 (2010).
- [17] M. H. S. Amin and V. Choi, First-order quantum phase transition in adiabatic quantum computation, *Phys. Rev. A* **80**, 062326 (2009).
- [18] N. G. Dickson and M. H. S. Amin, Does adiabatic quantum optimization fail for np-complete problems?, *Phys. Rev. Lett.* **106**, 050502 (2011).
- [19] E. Farhi, J. Goldstone, D. Gosset, S. Gutmann, H. B. Meyer, and P. Shor, *Quantum adiabatic algorithms, small gaps, and different paths* (2010), arXiv:0909.4766 [quant-ph].
- [20] M. Werner, A. García-Sáez, and M. P. Estarellas, Bounding first-order quantum phase transitions in adiabatic quantum computing, *Phys. Rev. Res.* **5**, 043236 (2023).
- [21] B. Kraus, H. P. Büchler, S. Diehl, A. Kantian, A. Micheli, and P. Zoller, Preparation of entangled states by quantum markov processes, *Phys. Rev. A* **78**, 042307 (2008).
- [22] S. Diehl, A. Micheli, A. Kantian, B. Kraus, H. Büchler, and P. Zoller, Quantum states and phases in driven open quantum systems with cold atoms, *Nature Physics* **4**, 878 (2008).
- [23] F. Verstraete, M. M. Wolf, and J. Ignacio Cirac, Quantum computation and quantum-state engineering driven by dissipation, *Nature physics* **5**, 633 (2009).
- [24] S. Diehl, E. Rico, M. A. Baranov, and P. Zoller, Topology by

- dissipation in atomic quantum wires, *Nature physics* **7**, 971 (2011).
- [25] C.-E. Bardyn, M. A. Baranov, C. V. Kraus, E. Rico, A. İmamoğlu, P. Zoller, and S. Diehl, Topology by dissipation, *New Journal of Physics* **15**, 085001 (2013).
- [26] J. C. Budich, P. Zoller, and S. Diehl, Dissipative preparation of chern insulators, *Phys. Rev. A* **91**, 042117 (2015).
- [27] M. Goldstein, Dissipation-induced topological insulators: A no-go theorem and a recipe, *SciPost Phys.* **7**, 067 (2019).
- [28] Z. Liu, E. J. Bergholtz, and J. C. Budich, Dissipative preparation of fractional chern insulators, *Phys. Rev. Res.* **3**, 043119 (2021).
- [29] F. Yang, P. Mognini, and E. J. Bergholtz, Dissipative boundary state preparation, *Phys. Rev. Res.* **5**, 043229 (2023).
- [30] S. Bandyopadhyay and A. Dutta, Dissipative preparation of many-body floquet chern insulators, *Phys. Rev. B* **102**, 184302 (2020).
- [31] L. Zhou, S. Choi, and M. D. Lukin, Symmetry-protected dissipative preparation of matrix product states, *Phys. Rev. A* **104**, 032418 (2021).
- [32] Y. Lin, J. Gaebler, F. Reiter, T. R. Tan, R. Bowler, A. Sørensen, D. Leibfried, and D. J. Wineland, Dissipative production of a maximally entangled steady state of two quantum bits, *Nature* **504**, 415 (2013).
- [33] F. Reiter, D. Reeb, and A. S. Sørensen, Scalable dissipative preparation of many-body entanglement, *Phys. Rev. Lett.* **117**, 040501 (2016).
- [34] M. J. Kastoryano, F. Reiter, and A. S. Sørensen, Dissipative preparation of entanglement in optical cavities, *Phys. Rev. Lett.* **106**, 090502 (2011).
- [35] V. Gorini, A. Kossakowski, and E. C. G. Sudarshan, Completely positive dynamical semigroups of n-level systems, *Journal of Mathematical Physics* **17**, 821 (1976).
- [36] G. Lindblad, On the generators of quantum dynamical semigroups, *Communications in mathematical physics* **48**, 119 (1976).
- [37] J. Dalibard, Y. Castin, and K. Mølmer, Wave-function approach to dissipative processes in quantum optics, *Phys. Rev. Lett.* **68**, 580 (1992).
- [38] M. B. Plenio and P. L. Knight, The quantum-jump approach to dissipative dynamics in quantum optics, *Rev. Mod. Phys.* **70**, 101 (1998).
- [39] A. J. Daley, Quantum trajectories and open many-body quantum systems, *Advances in Physics* **63**, 77 (2014).
- [40] J. P. Garrahan and I. Lesanovsky, Thermodynamics of quantum jump trajectories, *Phys. Rev. Lett.* **104**, 160601 (2010).
- [41] F. Carollo, R. L. Jack, and J. P. Garrahan, Unraveling the large deviation statistics of markovian open quantum systems, *Phys. Rev. Lett.* **122**, 130605 (2019).
- [42] W. Heiss, Exceptional points of non-hermitian operators, *Journal of Physics A: Mathematical and General* **37**, 2455 (2004).
- [43] M. V. Berry, Physics of nonhermitian degeneracies, *Czechoslovak journal of physics* **54**, 1039 (2004).
- [44] W. D. Heiss, The physics of exceptional points, *Journal of Physics A: Mathematical and Theoretical* **45**, 444016 (2012).
- [45] R. El-Ganainy, K. G. Makris, M. Khajavikhan, Z. H. Musslimani, S. Rotter, and D. N. Christodoulides, Non-hermitian physics and pt symmetry, *Nature Physics* **14**, 11 (2018).
- [46] Ş. K. Özdemir, S. Rotter, F. Nori, and L. Yang, Parity–time symmetry and exceptional points in photonics, *Nature materials* **18**, 783 (2019).
- [47] M.-A. Miri and A. Alu, Exceptional points in optics and photonics, *Science* **363**, eaar7709 (2019).
- [48] F. Minganti, A. Miranowicz, R. W. Chhajlany, and F. Nori, Quantum exceptional points of non-hermitian hamiltonians and liouvillians: The effects of quantum jumps, *Phys. Rev. A* **100**, 062131 (2019).
- [49] I. I. Arkhipov, A. Miranowicz, F. Minganti, and F. Nori, Liouvillian exceptional points of any order in dissipative linear bosonic systems: Coherence functions and switching between \mathcal{PT} and anti- \mathcal{PT} symmetries, *Phys. Rev. A* **102**, 033715 (2020).
- [50] F. Minganti, A. Miranowicz, R. W. Chhajlany, I. I. Arkhipov, and F. Nori, Hybrid-liouvillian formalism connecting exceptional points of non-hermitian hamiltonians and liouvillians via postselection of quantum trajectories, *Phys. Rev. A* **101**, 062112 (2020).
- [51] S. Khandelwal, N. Brunner, and G. Haack, Signatures of liouvillian exceptional points in a quantum thermal machine, *PRX Quantum* **2**, 040346 (2021).
- [52] W. Chen, M. Abbasi, Y. N. Joglekar, and K. W. Murch, Quantum jumps in the non-hermitian dynamics of a superconducting qubit, *Phys. Rev. Lett.* **127**, 140504 (2021).
- [53] J.-W. Zhang, J.-Q. Zhang, G.-Y. Ding, J.-C. Li, J.-T. Bu, B. Wang, L.-L. Yan, S.-L. Su, L. Chen, F. Nori, *et al.*, Dynamical control of quantum heat engines using exceptional points, *Nature communications* **13**, 6225 (2022).
- [54] W. Chen, M. Abbasi, B. Ha, S. Erdamar, Y. N. Joglekar, and K. W. Murch, Decoherence-induced exceptional points in a dissipative superconducting qubit, *Phys. Rev. Lett.* **128**, 110402 (2022).
- [55] Y.-L. Zhou, X.-D. Yu, C.-W. Wu, X.-Q. Li, J. Zhang, W. Li, and P.-X. Chen, Accelerating relaxation through liouvillian exceptional point, *Phys. Rev. Res.* **5**, 043036 (2023).
- [56] J.-T. Bu, J.-Q. Zhang, G.-Y. Ding, J.-C. Li, J.-W. Zhang, B. Wang, W.-Q. Ding, W.-F. Yuan, L. Chen, i. m. c. K. Özdemir, F. Zhou, H. Jing, and M. Feng, Enhancement of quantum heat engine by encircling a liouvillian exceptional point, *Phys. Rev. Lett.* **130**, 110402 (2023).
- [57] F. Minganti, A. Biella, N. Bartolo, and C. Ciuti, Spectral theory of liouvillians for dissipative phase transitions, *Phys. Rev. A* **98**, 042118 (2018).
- [58] D. A. Lidar, I. L. Chuang, and K. B. Whaley, Decoherence-free subspaces for quantum computation, *Phys. Rev. Lett.* **81**, 2594 (1998).
- [59] S. McArdle, T. Jones, S. Endo, Y. Li, S. C. Benjamin, and X. Yuan, Variational ansatz-based quantum simulation of imaginary time evolution, *npj Quantum Information* **5**, 75 (2019).
- [60] H. Nishi, T. Kosugi, and Y.-i. Matsushita, Implementation of quantum imaginary-time evolution method on nisq devices by introducing nonlocal approximation, *npj Quantum Information* **7**, 85 (2021).
- [61] A. Lucas, Ising formulations of many np problems, *Frontiers in physics* **2**, 5 (2014).
- [62] See the supplemental material for details.
- [63] The steady state corresponding to a unsatisfiable 3SAT instance is generally a complicated mixed state.
- [64] W. Barthel, A. K. Hartmann, M. Leone, F. Ricci-Tersenghi, M. Weigt, and R. Zecchina, Hiding solutions in random satisfiability problems: A statistical mechanics approach, *Phys. Rev. Lett.* **88**, 188701 (2002).
- [65] When λ_0 and λ_1 in Fig. 2(a) cross at $W = W_c$, we keep denoting the eigenvalue of the solution state $|\psi_{\text{sol}}\rangle \langle \psi_{\text{sol}}|$ with λ_0 for simplicity. This convention keeps Eq. (5) valid at both $W > W_c$ and $W < W_c$ without exchanging basis vectors.
- [66] C. M. Bender and S. Boettcher, Real spectra in non-hermitian hamiltonians having PT symmetry, *Phys. Rev. Lett.* **80**, 5243 (1998).

- [67] C. M. Bender, M. Berry, and A. Mandilara, Generalized pt symmetry and real spectra, *Journal of Physics A: Mathematical and General* **35**, L467 (2002).
- [68] A. Mostafazadeh, Pseudo-hermiticity versus pt symmetry: The necessary condition for the reality of the spectrum of a non-hermitian hamiltonian, *Journal of Mathematical Physics* **43**, 205 (2002).
- [69] A. Mostafazadeh, Pseudo-hermiticity versus pt -symmetry. ii. a complete characterization of non-hermitian hamiltonians with a real spectrum, *Journal of Mathematical Physics* **43**, 2814–2816 (2002).
- [70] F. Carollo, A. Lasanta, and I. Lesanovsky, Exponentially accelerated approach to stationarity in markovian open quantum systems through the mpemba effect, *Phys. Rev. Lett.* **127**, 060401 (2021).
- [71] I. Affleck, T. Kennedy, E. H. Lieb, and H. Tasaki, Rigorous results on valence-bond ground states in antiferromagnets, *Phys. Rev. Lett.* **59**, 799 (1987).
- [72] Y. Wang, K. Snizhko, A. Romito, Y. Gefen, and K. Murch, Dissipative preparation and stabilization of many-body quantum states in a superconducting qutrit array, *Phys. Rev. A* **108**, 013712 (2023).
- [73] X.-K. Gu, L.-Z. Tan, F. Nori, and J. Q. You, *Exploring dynamics of open quantum systems in naturally inaccessible regimes* (2025), arXiv:2503.06946 [quant-ph].

Supplemental material for “Asymptotic Exceptional Steady States in Dissipative Dynamics”

Yu-Min Hu¹ and Jan Carl Budich^{1,2,*}

¹Max Planck Institute for the Physics of Complex Systems, Nöthnitzer Str. 38, 01187 Dresden, Germany

²Institute of Theoretical Physics, Technische Universität Dresden and
Würzburg-Dresden Cluster of Excellence ct.qmat, 01062 Dresden, Germany

I. CLASSICAL DYNAMICS IN DISSIPATIVE 3SAT SOLVER

In this section, we show that the dissipative 3SAT solver discussed in the main text can be reduced to a classical dynamics. In the main text, we consider the Lindblad master equation with $H = 0$ and $L_{m,\alpha} = \sigma_{m_\alpha}^x P_m$ where $\alpha = 1, 2, 3$. Given that $\sigma_{m_\alpha}^x (1 \pm \sigma_{m_\alpha}^z)/2 = \sigma_{m_\alpha}^\mp$, $L_{m,\alpha} \rho L_{m,\alpha}^\dagger$ only has nontrivial actions on the diagonal part of the reduced density matrix for the qubits involved in clause C_m . This indicates that the dissipative dynamics decouples the diagonal and off-diagonal parts of the density matrix. Therefore, in the computational basis where the solution state to a satisfiable instance is just a basis vector, we focus on the classical dynamics occurring between the diagonal elements of the density matrix and focus on the relaxation to the solution state.

To proceed, we denote the diagonal operator subspace of the n th qubit as

$$|\uparrow_n\rangle = |\uparrow_n\rangle\langle\uparrow_n|, \quad |\downarrow_n\rangle = |\downarrow_n\rangle\langle\downarrow_n|. \quad (1)$$

We also denote the classical actions in the diagonal operator subspace as

$$\begin{aligned} \Sigma_n^x |\uparrow_n\rangle &= |\downarrow_n\rangle, & \Sigma_n^x |\downarrow_n\rangle &= |\uparrow_n\rangle, \\ \Sigma_n^z |\uparrow_n\rangle &= |\uparrow_n\rangle, & \Sigma_n^z |\downarrow_n\rangle &= -|\downarrow_n\rangle. \end{aligned} \quad (2)$$

With these notations, we represent the diagonal elements of the density matrix ρ in the qubit computation basis as a classical probability distribution among the corresponding classical bit strings:

$$p_i = \langle i|\rho|i\rangle \in [0, 1], \quad (3)$$

where $|i\rangle$ takes from 2^N computational basis vectors. They form a 2^N -component real vector \vec{p} . As a result, the Lindblad master equation for Eq.(3) of the main text leads to the vector \vec{p} following a classical evolution $\frac{d\vec{p}}{dt} = \mathcal{M}_W \vec{p}$ with the generator given by

$$\mathcal{M}_W = \sum_{m=1}^M \sum_{\alpha=1}^3 (W \Sigma_{m_\alpha}^x - 1) \mathcal{P}_m. \quad (4)$$

Here, \mathcal{P}_m is the analogous projector on the diagonal basis. For example, $C_m = x_{m_1} \vee \neg x_{m_2} \vee x_{m_3}$ corresponds to $\mathcal{P}_m = (1 - \Sigma_{m_1}^z)(1 + \Sigma_{m_2}^z)(1 - \Sigma_{m_3}^z)/8$. The physical classical Markovian

dynamics is given by $W = 1$, where the sum of each column of \mathcal{M}_1 is equal to zero and the total probability $\sum_{i=1}^{2^N} p_i = \text{Tr}[\rho] = 1$ is conserved.

The classical dynamical generator \mathcal{M}_W allows us to obtain numerical results for a relatively large system size. Practically, we exactly diagonalize \mathcal{M}_W to obtain the numerical data in Figs. 1 and 2 of the main text.

II. GENERATING SATISFIABLE 3SAT INSTANCES

The numerical results in the main text require the generation of random satisfiable and hard-to-solve 3SAT instances. Given the number of variables N , we generate $M = \text{round}(\alpha_c N)$ clauses for each instance. The parameter $\alpha_c \approx 4.267$ is the satisfiability threshold for the 3SAT problem [1]. Below this critical value, most random 3SAT instances tend to be satisfiable; above it, they are overwhelmingly unsatisfiable. The instances near this critical value are the most computationally challenging ones.

In this paper, we require all the generated 3SAT instances to be satisfiable. This is done by the method developed in Ref. [2] with a parameter $p_0 = 0.08$. This method generates satisfiable hard instances with at least one solution. We then only select instances with a unique solution for the numerical investigation in the main text. We also keep instances with two solutions for the numerical investigation in Sec. IV of this supplemental material.

Before closing this section, we remark that the specific instances used in Fig. 1, Fig. 2(a,b,c), and Fig. 3(b) in the main text are employed as examples. The critical values W_c in Fig. 2(c) and Fig. 3(b) are also determined for each instance. Nevertheless, the instance-dependent results shown in these plots are qualitatively the same for different instances.

III. THE SPECTRUM OF THE LEFT EIGENOPERATOR FOR THE METASTABLE STATE.

In the main text, we mentioned that, for the dissipative 3SAT solver at $W = 1$, the left eigenoperators l_1 of metastable states are semidefinite with a single zero eigenvalue. In this section, we present the numerical evidence to support this point.

As discussed in the main text, the left and right eigenoperators of the metastable state are labeled by l_1 and r_1 , respectively. Since we take the normalization of r_1 as $\text{Tr}[r_0^\dagger r_1] = 1$ where $r_0 = |\psi_{\text{sol}}\rangle\langle\psi_{\text{sol}}|$ is the unique steady state of \mathcal{L}_1 , the normalization of l_1 is fixed by $\text{Tr}[l_1^\dagger r_1] = 1$. As shown in the

* jan.budich@tu-dresden.de

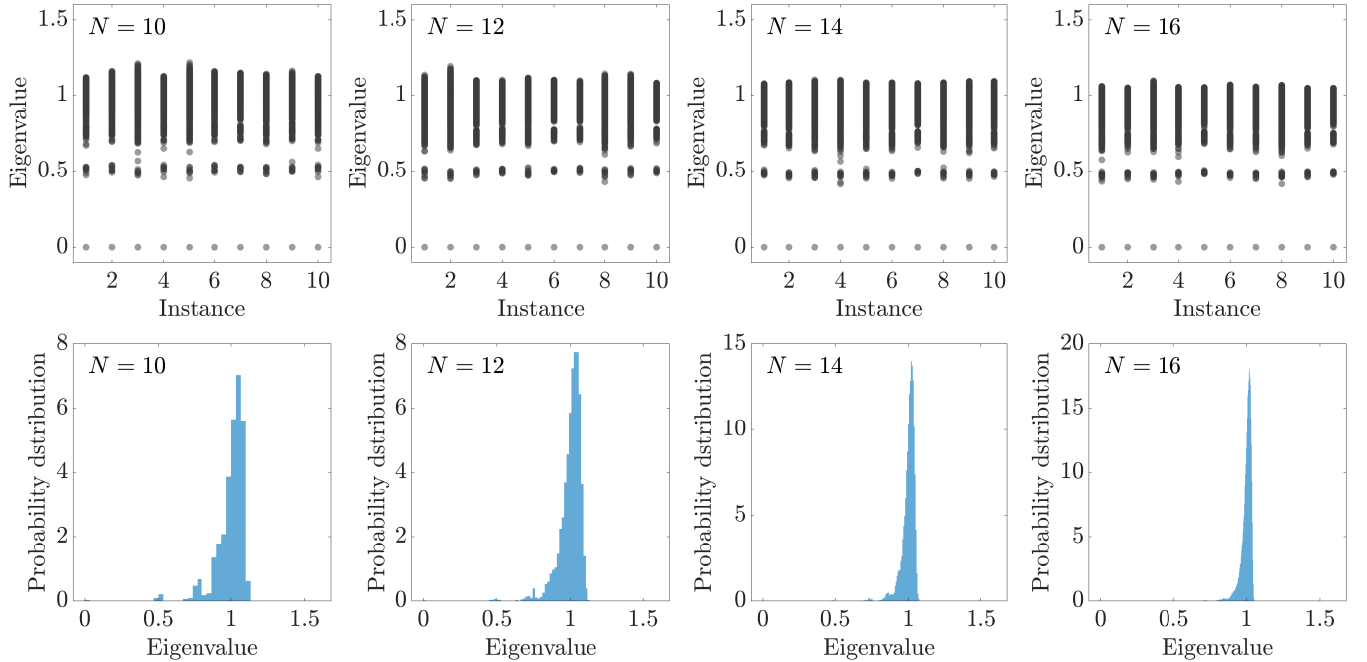


FIG. 1. Top: The eigenvalues of $\kappa^{-1}l_1$ for ten typical satisfiable 3SAT instances with a unique solution. Bottom: the probability distribution function of eigenvalues of the first instance in the top row. Each column corresponds to a specific variable number N , which is shown in each plot. We consider the physical case $W = 1$.

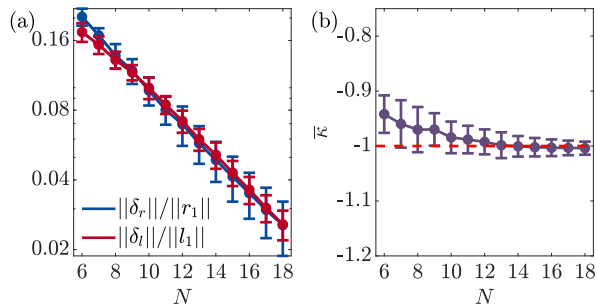


FIG. 2. (a) The averaged relative norm of the small corrections δ in r_1 and l_1 . (b) The mean value of κ . The red dashed line represents $\kappa = -1$. Each point is averaged over 10^3 satisfiable instances, with the error bar implying the standard deviation among different instances. Each instance is selected to have one unique solution. We consider the physical case $W = 1$.

main text, the left eigenoperator l_1 is given by $l_1 = \kappa(I - r_0) + \delta_l$ with $\kappa = \text{Tr}[l_1]/(2^N - 1)$ and $\frac{\|\delta_r\|}{\|r_1\|} \rightarrow 0$. Additionally, the eigenvalue λ_1 of the metastable state is observed to be real, indicating that l_1 is Hermitian [3]. As a result, to show the semi-definiteness of l_1 , we demonstrate that the eigenvalues of $\kappa^{-1}l_1$ for different instances are nonnegative, and have a constant gap above a single zero eigenvalue.

The numerical results of the eigenvalues of $\kappa^{-1}l_1$ for different instances are shown in Fig. 1. We find that there is a single zero eigenvalue of each $\kappa^{-1}l_1$, whose eigenstate corresponds to $|\psi_{\text{sol}}\rangle$. Other eigenvalues of $\kappa^{-1}l_1$ are positive. These results indicate that $\kappa^{-1}l_1$ is positive semidefinite. Interest-

ingly, except for a few modes, most eigenvalues are centered around 1, indicating that $\kappa^{-1}l_1$ is close to the extensive projector $I - |\psi_{\text{sol}}\rangle\langle\psi_{\text{sol}}|$.

In Fig. 2, we present more numerical data to better illustrate the structure of r_1 and l_1 . As discussed in the main text, $r_1 = r_0 + \delta_r$ and $l_1 = \kappa(I - r_0) + \delta_l$. Fig. 2(a) shows that the mean value of $\frac{\|\delta_r\|}{\|r_1\|}$ and $\frac{\|\delta_l\|}{\|l_1\|}$ among different satisfiable 3SAT instances exhibits an exponential decay, which is consistent with the analysis of the eigenoperator structure in the main text. Additionally, Fig. 2(b) demonstrates that $\kappa = \text{Tr}[l_1]/(2^N - 1)$ converges to -1 with the increase of variable number N . This numerical finding, together with the eigenvalue concentration of $\kappa^{-1}l_1$ shown in Fig. 1 and the smallness of $\frac{\|\delta_l\|}{\|l_1\|}$ shown in Fig. 2(a), indicates that l_1 is very close to $r_0 - I$ in the operator space.

IV. DEGENERATE STEADY STATES

In the main text, we focus on the asymptotic exceptional steady state (AESS) in classical and quantum systems that have a unique steady state. This section demonstrates that AESS can coexist with multiple steady states, and that our focus on uniquely solvable 3SAT instances in the main text does not lead to a loss of generality.

When a Liouvillian $\mathcal{L}_{W=1}$ has more than one steady state, the spectral decomposition $\mathcal{L}_1[r_i] = \lambda_i r_i$ and $\mathcal{L}_1^\dagger[l_i] = \lambda_i^* l_i$ gives rise to $\lambda_0 = \lambda_1 = \dots = \lambda_{d-1} = 0$ where d is the degeneracy of steady states. The d eigenoperators $\{r_0, r_1, \dots, r_{d-1}\}$ in the steady-state subspace of \mathcal{L}_1 are linearly independent and

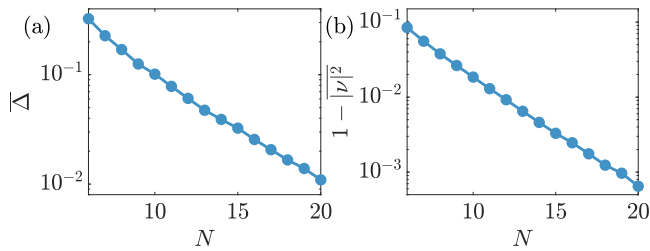


FIG. 3. The mean dissipative gap $\bar{\Delta}$ and eigenoperator overlap $1 - |\nu|^2$ at $W = 1$ for 3SAT instances with two distinct satisfiable solutions. Each data point is obtained by diagonalizing \mathcal{M}_1 and averaging over 10^3 random instances. For each variable number N , $M = \text{round}(\alpha_c N)$ and $\alpha_c \approx 4.267$.

form a d -dimensional subspace [3]. Namely, they cannot form any EP subspace by themselves. We can employ the Gram-Schmidt decomposition to construct an orthonormal operator basis based on these d eigenoperators. For simplicity, we assume that this step has been done and $\{r_0, r_1, \dots, r_{d-1}\}$ are orthogonal to each other.

Other modes correspond to $0 > \text{Re}(\lambda_d) \geq \text{Re}(\lambda_{d+1}) \geq \text{Re}(\lambda_{d+2}) \geq \dots$. We do not consider the situation with purely imaginary eigenvalues, although the analysis below can also apply to that case by tracking the eigenmodes whose eigenvalue asymptotically approaches zero in the thermodynamic limit.

Similar to the main text, we define the Liouvillian gap as

$$\Delta = -\text{Re}(\lambda_d). \quad (5)$$

The eigenstate overlap is defined between the metastable state r_d and the steady-state subspace spanned by the orthogonal basis $\{r_0, r_1, \dots, r_{d-1}\}$. With the normalized eigenoperator $\hat{r}_i = r_i / \|r_i\|$, we have the following definition:

$$|\nu|^2 = \sum_{k=0}^{d-1} |\text{Tr}[\hat{r}_d^\dagger \hat{r}_k]|^2. \quad (6)$$

Therefore, we can expect that the AESS coexists with multiple steady states when both Δ and $1 - |\nu|^2$ approach zero as the system size increases. In this case, the metastable state can have a large overlap with a particular state in the steady-state subspace, while keeping orthogonal to other states.

As an example, we consider the classical dynamics introduced in Eq.(4) for 3SAT instances with two different satisfiable solutions $|\psi_{\text{sol},1}\rangle$ and $|\psi_{\text{sol},2}\rangle$. By definition, $|\psi_{\text{sol},1}\rangle$ and $|\psi_{\text{sol},2}\rangle$ are just two classical states in the computational basis to represent the two bit configurations that solve the given instance. Since our classical dynamics only involves the diagonal parts of the density matrix, the corresponding two steady states of \mathcal{M}_1 are $r_0 = |\psi_{\text{sol},1}\rangle \langle \psi_{\text{sol},1}|$ and $r_1 = |\psi_{\text{sol},2}\rangle \langle \psi_{\text{sol},2}|$ [4]. Therefore, $\Delta = -\text{Re}(\lambda_2)$ and $|\nu|^2 = |\langle \psi_{\text{sol},1} | \hat{r}_2 | \psi_{\text{sol},1} \rangle|^2 + |\langle \psi_{\text{sol},2} | \hat{r}_2 | \psi_{\text{sol},2} \rangle|^2$. The mean quantities $\bar{\Delta}$ and $1 - |\nu|^2$, averaged over 10^3 random 3SAT instances with two satisfiable solutions, are shown in Fig.3. These two quantities display an exponential decay as the system size increases, similar to Fig.1 of the main text. These results demonstrate that the AESS can coexist with multiple steady states.

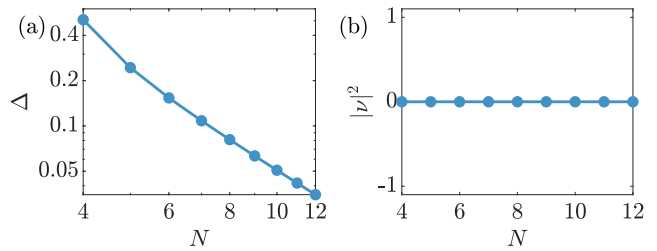


FIG. 4. The Liouvillian gap Δ (a) and the eigenoperator overlap $|\nu|^2$ (b) for the dephasing XX chain \mathcal{L}_1 defined in Sec. V A.

V. EXAMPLES WITHOUT ASYMPTOTIC EXCEPTIONAL STEADY STATES

In the main text and the previous section of the supplemental material, we mainly focus on classical and quantum systems with AESS. In this section, we show two examples without AESS, where only one of the limits $\lim_{N \rightarrow \infty} \Delta = 0$ and $\lim_{N \rightarrow \infty} |\nu|^2 = 1$ can be satisfied in the thermodynamic limit.

A. $\lim_{N \rightarrow \infty} \Delta = 0$ and $\lim_{N \rightarrow \infty} |\nu|^2 \neq 1$

We use a dephasing XX chain as an example in this case. The Hamiltonian is given by $H = \sum_{n=1}^{N-1} s_n^x s_{n+1}^x + s_n^y s_{n+1}^y$ and the jump operators are dephasing operators $L_n = s_n^z$. We take a unit damping rate. Here we consider open boundary conditions for a spin- $\frac{1}{2}$ chain with N spins. The total Liouvillian at $W = 1$ is given by $\mathcal{L}_1[\rho] = -i[H, \rho] + \sum_{n=1}^N L_n \rho L_n^\dagger - \frac{1}{2} \{L_n^\dagger L_n, \rho\}$. This open quantum system has a strong global $U(1)$ symmetry such that the total magnetization $S^z = \sum_{n=1}^N s_n^z$ is conserved. Meanwhile, since $L_n = L_n^\dagger$ is a Hermitian operator, the steady state for \mathcal{L}_1 is the identity operator in each symmetry sector labeled by the eigenvalues of S^z .

The eigenvalues and eigenoperators of \mathcal{L}_1 can be obtained in each symmetry sector. We perform exact diagonalization in the sector $S^z = 0$ for even spins and in the sector $S^z = -\frac{1}{2}$ for odd spins. Fig. 4 shows the numerical data for the Liouvillian gap Δ and eigenoperator overlap ν between the steady state and the slowest damping mode in these sectors. These results show that the Liouvillian gap algebraically decays to zero with the increase of the system size. However, the eigenoperator overlap ν remains zero, indicating that the steady state and the slowest damping mode are orthogonal to each other under Hilbert-Schmidt inner product. The zero overlap is expected here. The right eigenoperators of \mathcal{L}_1 with nonzero eigenvalues are traceless, and therefore, orthogonal to the steady state which is an identity matrix. The results in Fig. 4 suggest that a gapless Liouvillian with Hermitian jump operators cannot yield an AESS in the thermodynamic limit.

B. $\lim_{N \rightarrow \infty} \Delta \neq 0$ and $\lim_{N \rightarrow \infty} |\nu|^2 = 1$

The second example is a 1D classical Markovian dynamics for N classical bits. The generator is $\mathcal{M}_W = \sum_{n=1}^N (W \Sigma_n^x +$

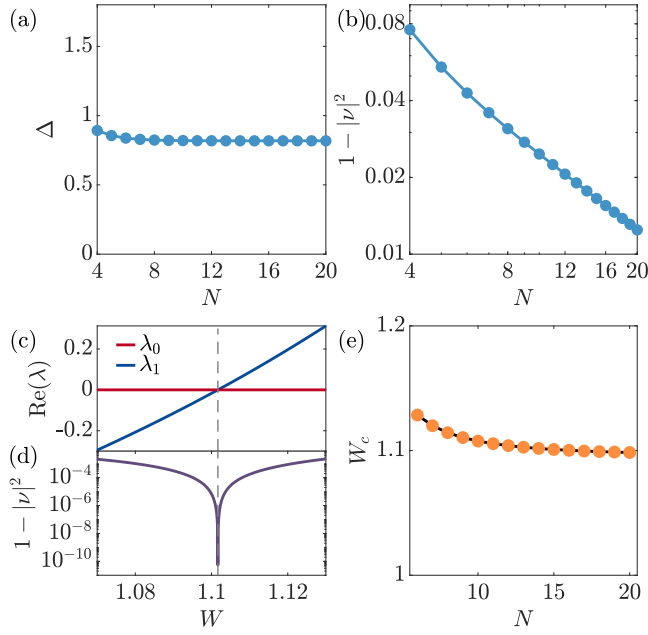


FIG. 5. The Liouvillian gap Δ (a) and the eigenoperator overlap $|v|^2$ (b) for a classical spin chain in Sec. VB at the physical point $W = 1$. (c) and (d) show the W -dependent Liouvillian gap Δ and eigenoperator overlap $|v|^2$ for $N = 14$. an exact EP appears at the critical value $W_c = 1.10167$. (e) The critical value W_c for different system sizes N . The black curve is fitted by $W_c = 1.0546N^{-1.9281} + 1.0952$, indicating a finite distance to the physical point $W = 1$ in the thermodynamic limit.

$W\Sigma_{n+1}^x - 2)(1 - \mathcal{P}_{n,n+1}^{\downarrow\downarrow})$. These notations are taken from Sec. I of this supplemental material. $\mathcal{P}_{n,n+1}^{\downarrow\downarrow} = |\downarrow\downarrow\rangle\langle\downarrow\downarrow|$ is a projection superoperator of two aligned neighboring spins in the downward direction. We consider the periodic boundary condition

here. By the construction, the steady state of this classical Markovian dynamics is given by the classical ferromagnetic state where all spins are downwards. It is a trivial task to prepare such a state.

Fig. 5 shows the dissipative gap Δ and the eigenoperator overlap v between the steady state and the slowest decay mode of \mathcal{M}_1 . The dissipative gap Δ is nearly constant, not decaying as the system size increases. In contrast, $1 - |v|^2$ exhibits a power-law decay with the increase of the system size. According to $\mathcal{L}_W^{\text{eff}}$ in the main text, we can write down an effective dynamical generator in the orthonormal basis constructed by the steady state and the slowest decay mode of \mathcal{M}_1 :

$$\mathcal{M}_1^{\text{eff}} = \begin{pmatrix} 0 & -\Delta \frac{v}{\sqrt{1-|v|^2}} \\ 0 & -\Delta \end{pmatrix}. \quad (7)$$

A finite gap $\Delta \neq 0$ indicates that $\mathcal{M}_1^{\text{eff}}$ will not asymptotically become an EP as the system size increases. Nevertheless, the two eigenoperators asymptotically become parallel to each other in the thermodynamic limit. We can express $\mathcal{M}_1^{\text{eff}}$ as

$$\mathcal{M}_1^{\text{eff}} = -\Delta \frac{v}{\sqrt{1-|v|^2}} \begin{pmatrix} 0 & 1 \\ 0 & \frac{1}{v} \end{pmatrix}. \quad (8)$$

As the system size increases, this matrix looks like an asymptotic Jordan block multiplied with a divergent prefactor.

We stress that this situation differs from AESS in the main text. The latter case, manifesting as both Δ and $1 - |v|^2$ vanishing in the thermodynamic limit, stays close to an exact EP at a critical value $W_c > 1$. The critical value W_c for AESS also converges to the physical point $W = 1$ in the thermodynamic limit. In contrast, although $\mathcal{M}_1^{\text{eff}}$ in Eq. (8) is also found to be near an exact EP at $W = W_c > 1$ [Figs. 5(c) and 5(d)], the critical value W_c remains a finite distance to the physical point $W = 1$ with the increase of the system size [Fig. 5(e)].

- [1] M. Mézard and R. Zecchina, Random k -satisfiability problem: From an analytic solution to an efficient algorithm, *Phys. Rev. E* **66**, 056126 (2002).
 [2] W. Barthel, A. K. Hartmann, M. Leone, F. Ricci-Tersenghi, M. Weigt, and R. Zecchina, Hiding solutions in random satisfiability problems: A statistical mechanics approach, *Phys. Rev.*

Lett. **88**, 188701 (2002).

- [3] F. Minganti, A. Biella, N. Bartolo, and C. Ciuti, Spectral theory of liouvillians for dissipative phase transitions, *Phys. Rev. A* **98**, 042118 (2018).
 [4] A full quantum consideration indicates that \mathcal{L}_1 has four steady states. The other two have an off-diagonal structure: $r_2 = |\psi_{\text{sol},1}\rangle\langle\psi_{\text{sol},2}|$ and $r_3 = |\psi_{\text{sol},2}\rangle\langle\psi_{\text{sol},1}|$.